Proceedings of the ASME 2009 Conference on Smart Materials, Adaptive Structures and Intelligent Systems
SMASIS2009
September 21-23, 2009, Oxnard, California, USA

SMASIS2009-1326

CRACK DETECTION AND MONITORING USING PASSIVE WIRELESS SENSOR

Srikar Deshmukh, University of Texas at Arlington

Irshad Mohammad, University of Texas at Arlington

Manos Tentzeris, Georgia Institute of Technology

Terence Wu, Georgia Institute of Technology

Haiying Huang, University of Texas at Arlington

ABSTRACT

This paper presents an antenna sensor that can detect and monitor crack remotely and passively. Since this antenna sensor does not need electric wires for power supply and data transmission, it has great potential to be implemented as large area sensor skin with high spatial resolution, simple configuration and remote-interrogation capability. The sensor fabrication, the sensor characterization procedure and the non-contact interrogation technique are presented. The experimental results demonstrated that the antenna sensor is sensitive to crack growth and can be interrogated remotely.

INTRODUCTION

Recent years have seen an increasing number of aircrafts that are operating beyond their design lives. Majority of these aging aircraft components will develop multiple fatigue cracks around geometry irregularities, dramatically reducing the fatigue strength of the aircrafts. Not only does the effect of multiple cracks on the structure integrity depend on the local stress state, it is also strongly influenced by the crack pattern and crack geometries. In order to predict the residual life cycle of these service components, detailed characterizations of the cracks are absolutely essential.

Different types of crack sensors have been developed to detect cracks indirectly based on the effect of cracks on the strain field, ultrasound wave propagation or vibration characteristics of the structure. Sensors based on RFID principle, piezoelectric materials and optical fiber sensors have been used extensively. The inductive coupling type of sensors has a very limited range of operation due to high coupling losses [1]. The crack sensors based on piezoelectric materials have low power efficiency and operate in a limited range of temperatures. In addition, most of these sensors are point sensors and their spatial resolution is limited due to the limited number of sensors can be deployed. To overcome this limitation, wireless sensor networks have been developed to collect and process the crack information at the sensor level, thus reducing the network load. These types of sensors require a power supply, thus increasing their cost, size and complexity [2, 3]. Optical fiber based sensor is a promising technology that can provide distributed strain sensing for crack detection with good spatial resolution. But optical fiber based sensors are expensive and delicate [4, 5].

This paper is focused on developing a passive wireless sensor that is capable of providing quantitative information about cracks on a metallic structure. Since this sensor does not require any power source, its shelf life and service life is virtually unlimited. The small size of the antenna sensor and its wireless nature enables its application in ultra-dense sensor networks that could achieve a sub-millimeter detection resolution. Monitoring the cracks using such a sensor network is expected to provide crucial information for structural health diagnosis and prognosis. Since this passive wireless sensor is extremely thin and conforms to most of the surfaces, it can be applied over any part of the structure requiring structural health monitoring. Other advantages of this passive wireless sensor include its low weight, low fabrication cost and high sensitivity.

PRINCIPLE OF OPERATION

The antenna sensor, shown in Figure 1, mainly comprises of a patch antenna mounted on a metallic structure, which acts as the ground plane for the patch antenna. The patch antenna is made up of a copper patch mounted on a flexible dielectric

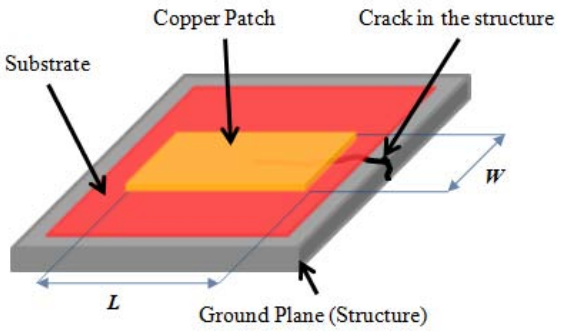

Figure 1: Antenna sensor description.

substrate. The copper patch and the ground plane form an electromagnetic resonant cavity, resonating at a specific frequency. For a rectangular patch antenna, there are two fundamental resonant frequencies, one frequency, f_{01}, dependent on the geometric length L of the copper patch and the other frequency, f_{10}, dependent on the geometric width (W) of the copper patch, as shown in Figure 1.

The resonant frequency of the antenna sensor is determined by the average length of the current path in the ground plane along the corresponding axis of the antenna sensor [6]. For example, the frequency f_{01} depends on the average length of the current path parallel to the geometric length L of the patch antenna. If a crack is perpendicular to the length of the patch antenna, the ground plane current paths tend to bend around the non-conductive region of the ground plane due to the presence of the crack. This causes the average length of the current path to increase, resulting in a reduction in the corresponding resonant frequency. Similarly, a crack perpendicular to the width of the patch antenna would cause the resonant frequency f_{10} to reduce. The magnitude of decrease in the resonant frequency is directly related to the crack length. Cracks also reduce the conductivity of ground plane and thus result in higher return losses.

FATIGUE SAMPLE FABRICATION AND PREPARATION

To characterize the antenna sensor's performance for crack monitoring, a Compact Tension (CT) specimen was designed and machined according to ASTM standards (E647-00) [7], as shown in Figure 2.a. Two screw holes were added at the edge of the CT specimen to facilitate the mounting of a SMA connector, which is needed to connect the antenna sensor to a Vector Network Analyzer (VNA) so that S_{11} parameters of the antenna sensor can be measured. The as-machined CT specimen, made of Al 7075-T6, was first subjected to 10 Hz fatigue cycling (P_{max} = 600 lb and R = 0.5) to introduce a precrack of 0.2 inches in length. After polishing the precracked CT specimen using 400, 600 and 1500 grit sand papers to remove the surface defects, a rectangular dielectric substrate (Kapton HN, 50 μm in thickness, 2in. x 1.5in) was placed next to the crack and was bonded to the specimen using superglue. To ensure a good bonding, the surfaces of the Kapton film were slightly sanded. A 66 μm thick copper strip (3M 118, 0.6 inches long and 0.5 inches wide) was then bonded on top of the Kapton film. The copper strip is oriented in such a way that the crack is aligned with the center line of its width direction and the crack tip is at a distance of 0.2 inches from the patch. This construction resulted in a highly flexible, low cost, rugged, and conformal antenna sensor. The antenna sensor can be excited contactly using a microstrip feed line or non-contactly using a horn antenna. For this experiment, we used the contact feeding method. A 1 mm wide microstrip feed line made of the copper film was bonded next to the copper patch. Conductive epoxy was dabbed on the patch/feed line interface to improve the conductivity between the patch and the feed line. An SMA connector was then mounted on the edge of the CT specimen

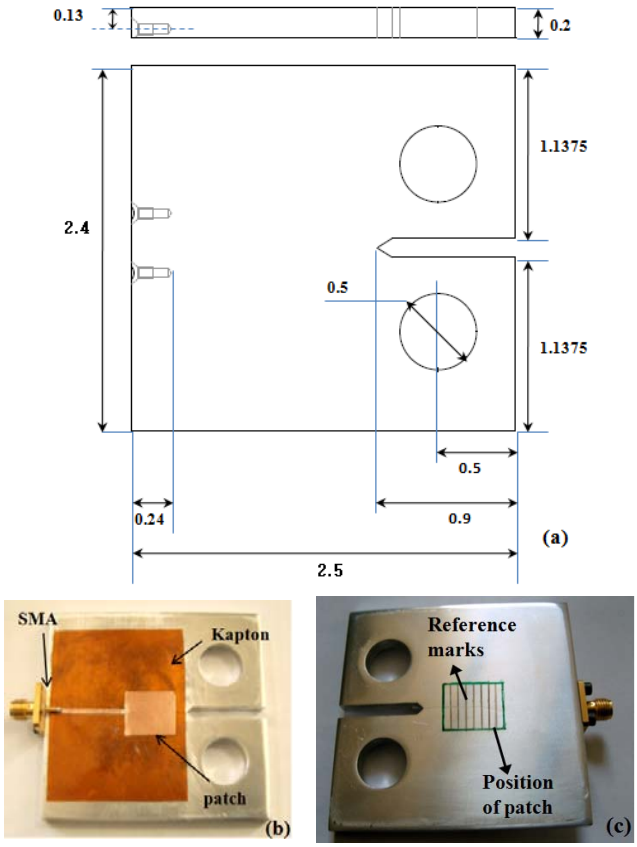

Figure 2: Fatigue specimen; (a) Specimen design (units in inches); (b) Antenna sensor and SMA assembly; (c) Reference marks on back side of specimen.

with its pin touching the end of the micro strip feed line. Figure 2.b shows the patch antenna and SMA connector assembly. The location of the antenna patch was marked on the other side of the CT specimen. To facilitate measuring the crack length using a digital camera, reference marks with a gap of 2 mm are also drawn on the specimen. A digital image of the CT specimen with the antenna patch position and the reference markers are shown in Figure 2.c. Marker 0 indicates the left edge of the antenna patch. After fabricating the antenna sensor on the CT

specimen, the S_{11} parameter of the antenna sensor was measured using a VNA. The antenna sensor displayed two resonant frequencies with f_{10} = 9.2 GHz and f_{10} = 6.3 GHz, as shown Figure 3. Since the crack is perpendicular to the width direction of the antenna patch, it is expected that f_{10} should shift to a lower value when the crack grows.

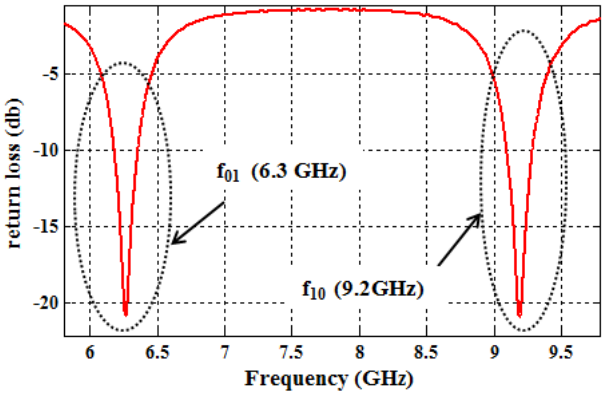

Figure 3: Resonant frequencies of patch antenna.

EXPERIMENTAL SETUP AND PROCEDURE

The experimental set up to propagate the crack is shown in Figure 4. The CT specimen was subjected to fatigue loading (5 Hz loading frequency, P_{max} = 600 lb and R = 0.5) using a closed loop servo-hydraulic MTS machine. During the fatigue process, the VNA was connected to the patch antenna via SMA connector and the S_{11} parameter of the antenna sensor was monitored in real time. A CCD camera was placed at the opposite side of the antenna sensor. The digital image acquired by a computer was displayed on a monitor to track the crack propagation. Whenever the crack reached a reference mark, the fatigue loading was paused at 300 lbs. The S_{11} parameter of the antenna sensor for that particular crack length was then recorded. After the measurement, the fatigue loading was resumed until the crack reached the next reference mark. The experiment was terminated when the crack spanned the entire length of the antenna patch.

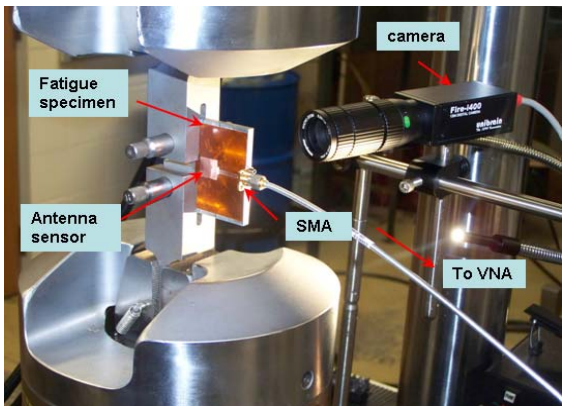

Figure 4: Experimental setup.

NON-CONTACT MEASUREMENT

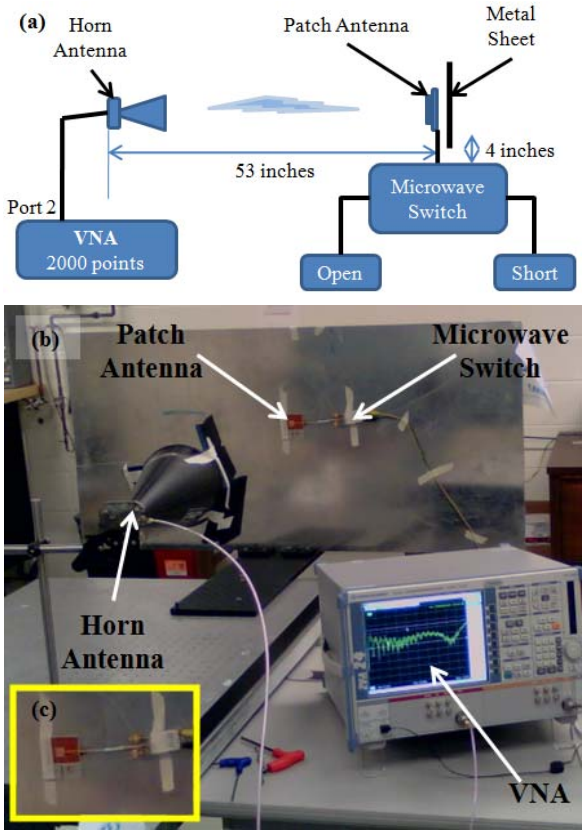

Figure 5: (a) Experimental setup description; (b) Actual experimental set up; (c) Patch antenna on a CT specimen.

Since the crack detection sensor described above is an antenna by itself, it can be interrogated wirelessly using a microwave radar system shown in Figure 5. A horn antenna is employed to irradiate the antenna sensor with a broadband Electromagnetic (EM) wave generated by the source of the Vector Network Analyzer (VNA). The antenna in turn scatters the EM signal back to the horn antenna. The backscattered signal comprises of two components: the antenna mode and the structure mode [8]. While the structure mode is due the backscattering from the structure components of the antenna, the antenna mode is due to the re-radiation of the signal received by the antenna due to mismatched antenna load. Therefore, the frequency spectrum of the antenna mode signal is directly related to the radiation characteristics of the patch antenna. By analyzing the antenna mode signal, the radiation parameters of the antenna sensor can be deciphered. However, the antenna mode backscattering is much smaller than the structural mode backscattering. When these two signals are received by the horn antenna indiscriminately, the spectrum displayed by the VNA is dominated by the structural mode signal, which makes extracting the spectrum of the antenna mode very difficult. In order to isolate the antenna mode from the backscattered signal, a microwave switch is connected to

the antenna sensor so that it can be switched from open-terminated to short-terminated. For these two impedance loads, the antenna mode signal has a 180 degree phase difference while the structural mode is the same [9, 10]. Therefore, by subtracting the backscattered signals at these two states, we can obtain an antenna mode signal whose amplitude is twice as that of the antenna mode signal at each state. In addition, the structural mode backscattering gets cancelled out by the subtraction.

The experimental implementation of the remote interrogation system is shown in Figure 5.b. The patch antenna sensor, similar to the one used in Figure 4, is placed in the far field region of the interrogating horn antenna (Singer - A6100), at a distance of 53 inches from the horn antenna. A large metal plate is placed behind the CT specimen to simulate a large metallic structure. The interrogating horn antenna is connected to one of the ports of a VNA (Rohde & Schwarz – ZVA24, 2 ports). The patch antenna is connected to the microwave switch (MSP2T-18, SPDT switch) using a 4 inch SMA cable, which switches the patch antenna to an open-termination when energized and short-termination when de-energized. Since the antenna sensor has two fundamental radiation modes, a dual polarization horn antenna is employed so that both antenna radiation modes can be measured by changing the polarization of the horn antenna to match the electrical field of the antenna radiation mode.

RESULTS AND DISCUSSIONS

The S_{11} curves of the antenna sensor at different crack lengths are shown in Figure 6.a. Position 0 indicates when the crack tip just reached the antenna patch. Each subsequent position increment is equivalent to 2 mm of crack growth. As expected, the f_{10} of the antenna sensor shifted towards lower frequencies as the crack length increased. To determine the sensitivity of the antenna sensor to the crack length, the resonant frequency shift of the antenna sensor is plotted versus the crack growth, as shown in Figure 6.b. The relationship between the resonant frequency shift and the crack growth appeared to be linear. Based on the linear fitting of the experimental data, the crack-growth sensitivity of the antenna sensor is estimated to be 29.6 MHz/mm. Considering that a VNA has a spectral resolution of 10 Hz, crack detection with a sub-millimeter resolution can be easily achieved using the antenna sensor.

The S_{11} parameter plot of the antenna sensor in Figure 5 was measured to characterize the patch antenna, as shown in Figure 7. The horn antenna was first polarized along the width of the patch antenna to measure the f_{10} frequency. The frequency domain backscatter signal acquired by the VNA was converted to time domain signal using Inverse Fast Fourier Transform (IFFT). The two time-domain backscatter signals acquired when the antenna sensor was open-terminated and short-terminated are shown in Figure 8.a and Figure 8.b respectively. Because these two signals are dominated by the structural mode, they looked almost identical. The wave packet at 0 ns is due to the internal reflections from the interrogating

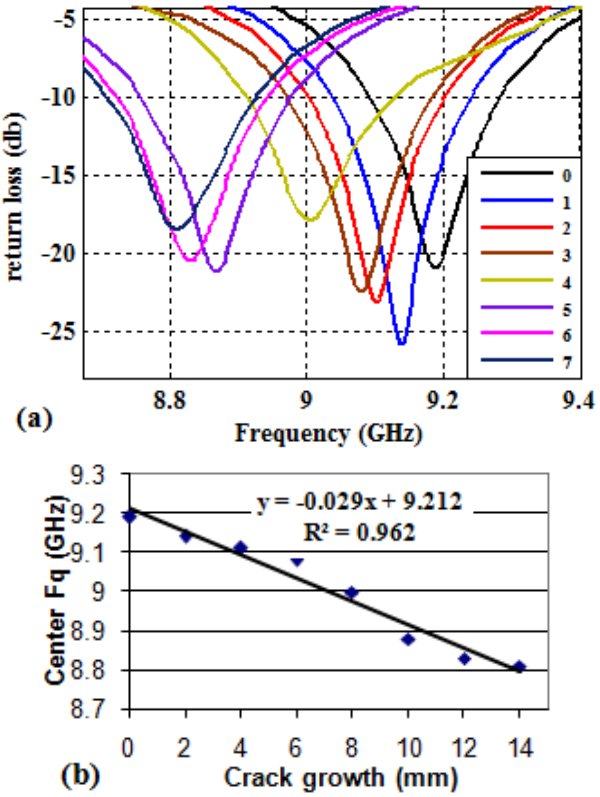

Figure 6: Resonant frequency shift and sensitivity of the antenna sensor; (a) S_{11} shifts with crack growth; (b) Crack growth vs. resonant frequency shift.

horn antenna. The large wave packet at 2 ns is due to the reflections from the VNA chassis. The third wave packet at 9 ns is due to the structure mode response of the patch antenna sensor and the large metallic structure. The small wave packet at 18 ns is due to the reflection from the wall. Antenna mode wave packet is too weak to be visible in Figure 8.

To distinguish the antenna mode from the structural model, the short-terminated signal is subtracted from the open-terminated signal to cancel out the structure mode. The normalized backscatter signal after subtraction, as shown in Figure 9, displayed a dominant wave packet at 10 ns. Because this time coincides with the time-of-flight for the EM signal to

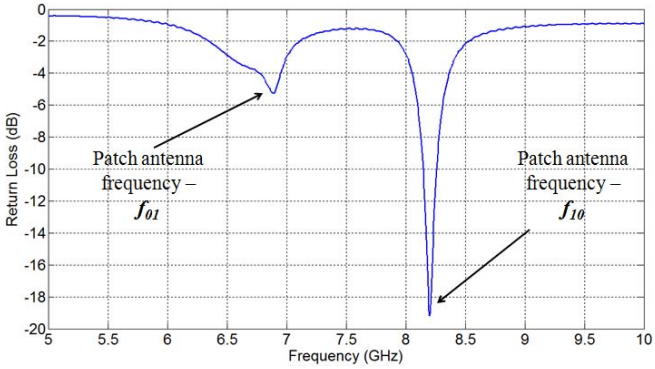

Figure 7: S_{11} response of patch antenna.

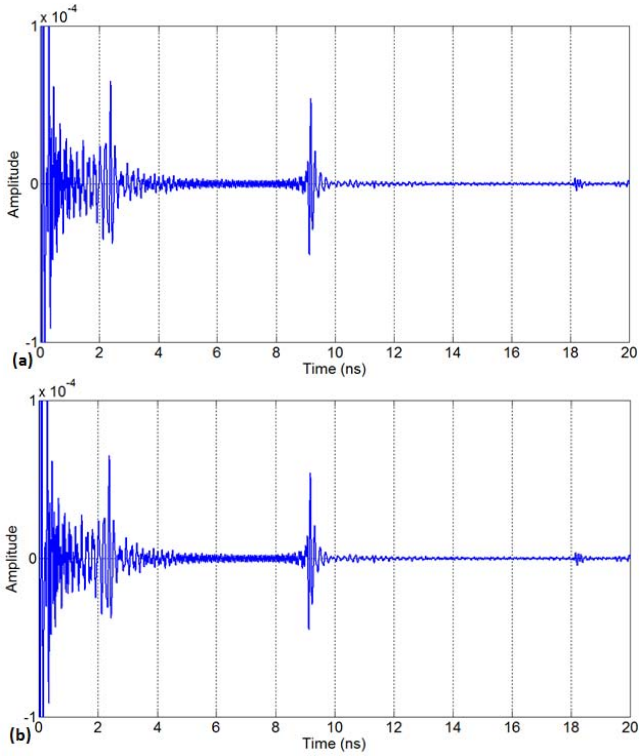

Figure 8: Backscatter signal; (a) with open circuit terminated patch antenna; (b) with short circuit terminated patch antenna.

travel from the horn antenna to the patch antenna load and back to the horn antenna, this wave packet may be the antenna mode signal. This is further confirmed by processing the normalized backscatter signal using Short Time Fourier Transform (STFT) and displaying the resulting spectrogram. As shown in Figure 10, the red-colored high intensity spot at 10 ns in time and at 8 GHz in frequency strongly indicates that the highlighted wave packet is indeed the antenna mode signal. Before applying Fast-Fourier Transformation to the normalized signal to obtain the spectrum of the antenna mode, the antenna mode signal was extracted from the normalized time domain signal using a rectangular window spanning from 9.81ns to 15.17ns. This time-gating operation improves the signal-to-noise ratio of the

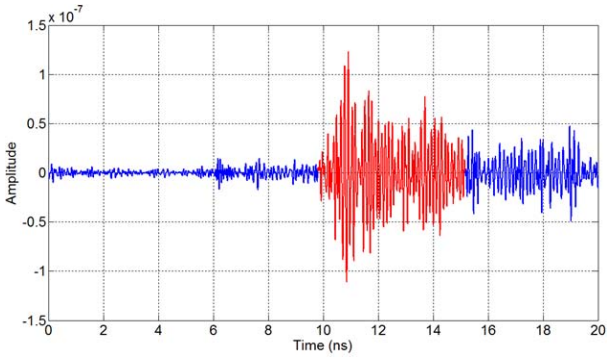

Figure 9: Normalized backscattered signal.

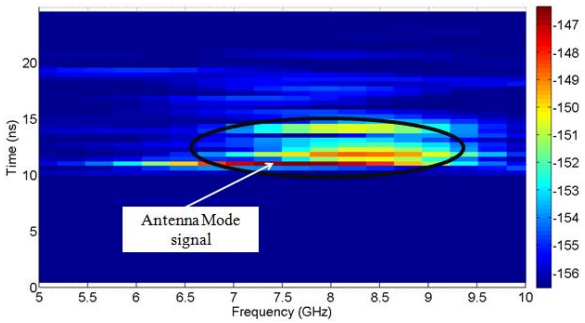

Figure 10: Spectrogram of the normalized backscatter signal.

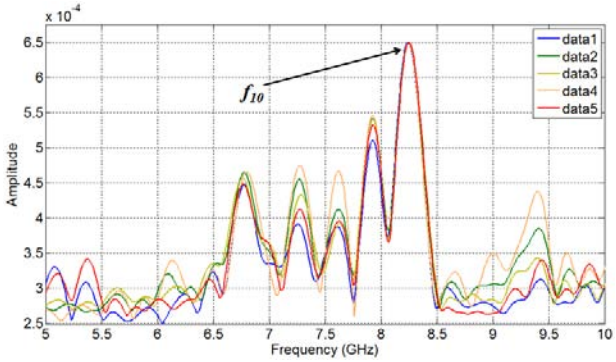

Figure 11: Frequency domain antenna mode signal after FFT processing – horn antenna polarized along the width of the patch antenna.

antenna mode spectrum by removing the irrelevant signal at other time period. The frequency spectrum of the time-gated antenna mode signal is shown in Figure 11. The resonant frequency of the patch antenna can be identified from this frequency spectrum as the frequency at which the amplitude peak is located. This frequency matches closely with that measured using S_{11} parameter of the patch antenna shown in Figure 7. The repeatability of the results over five measurements indicates that the measurement system is very stable and robust.

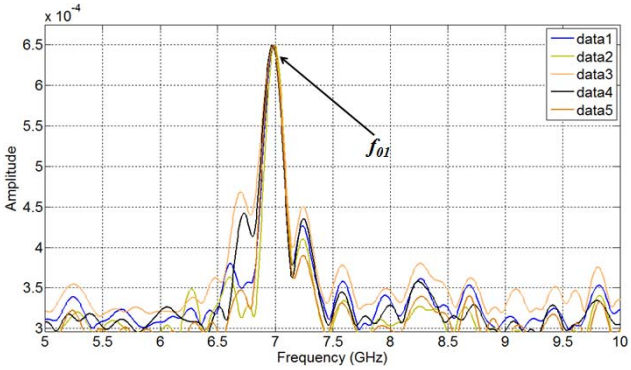

Figure 12: Frequency domain antenna mode signal after FFT processing – horn antenna polarized along the length of the patch antenna.

To measure the f_{01} resonant frequency, the interrogating horn antenna is aligned to be polarized along the length of the patch antenna. Again, the resonant frequency of the antenna sensor obtained using the non-contact method matched with that measured using S_{11} parameter of the antenna sensor very well, as shown in Figure 12.

FUTURE WORK

The microwave switch used for normalization in this paper requires a control voltage of 24 V. It can be replaced by a compact low voltage switching circuit that uses a high frequency Pseudomorphic High Electron Mobility Transistor (pHEMT), as shown in Figure 13. The pHEMT will be switched using a photocell. These two devices will be mounted on the same substrate as the patch antenna. The antenna sensor will be connected to the pHEMT using a microstrip transmission line.

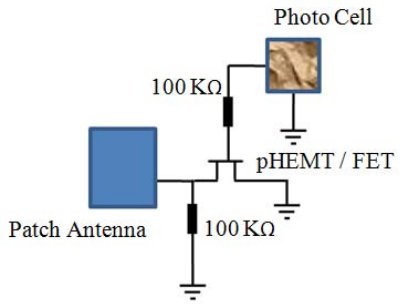

Figure 13: Compact normalization switching circuit.

The principle of normalization is similar to that of the microwave switch normalization as described in this paper. At normal state, i.e. when the photo cell is not illuminated, the pHEMT is on. In this state, its drain – source junction of the pHEMT acts as a short circuit. Thus the patch antenna is short - terminated. When the photo cell is illuminated with a LASER, a small voltage is generated. This voltage drives the pHEMT gate – source junction to turn the pHEMT off. In this state, the drain – source junction of the pHEMT acts as an open circuit. Thus the patch antenna is effectively open - terminated. Parallel high impedance resistors of 100kΩ will be placed in the circuit to block microwave signals from entering the DC bias. By switching the LASER, we can remotely control the patch antenna termination impedance and thus achieve normalization by non-contact means.

CONCLUSIONS

This paper presented the experimental work that proved the feasibility of using patch antennas for crack detection and monitoring. The non-contact measurement method enabled the antenna sensor to function wirelessly and passively, thus qualifying this antenna sensor as a passive wireless crack sensor.

ACKNOWLEDGMENTS

This project is supported by the Air Force Office of Scientific Research under contract No. FA9550-08-1-0317. The support and encouragement of program manager, Dr. Victor Giurgiutiu, is greatly appreciated.

REFERENCES

[1] Butler, J. C., Vigliotti, A. J., Verdi, F. W., Walsh, S. M., 2002, "Wireless, resonant-circuit, inductively coupled, inductive strain sensor", *Sensors and Actuators*, **A102**, pp. 61-66.

[2] Kiremidjian, G. K., Kiremidjian, A., and Lynch, J. P., 2004, "Wireless structural monitoring for homeland security applications", *Proc. of SPIE*, **5395**, pp. 82-90.

[3] Kurata, N., Spencer, B. F. and Ruiz-Sandavol, M.., 2005, "Risk monitoring of buildings with wireless sensor networks", *Struct. Cont. and Health Monit.*, **12**, pp. 315-327.

[4] Liu, Y., Lacher, A., Wang, G., Purekar, A. and Yu, M., 2007, "Wireless fiber optic sensor system for strain and pressure measurements on a rotor blade", *Proc. of SPIE* **6770** 67700Y.

[5] Murphy, K. A. and Poland, S. H., 1997, "Fiber optic strain and pressure sensors", *Proc. of SPIE* **3044**, pp. 352-358.

[6] Byun, S., Lee, J., Lim, J., and Yun, T., 2007, "Reconfigurable ground-slotted patch antenna using PIN diode switching", *ETRI journal*, **29**(6), pp. 832-834.

[7] Standard Test Method for Measurement of Fatigue Crack Growth Rates, ASTM standards, E 647-00.

[8] Penttila, K., Keskilammi, M., Sydanheimo, L., and Kivikoski, M., 2006, "Radar cross-section analysis for passive RFID systems", *IEE Proc.–Microwave Antennas Propagation*, **153**(1), pp. 103- 109.

[9] Hu, S., Lay, C., Shen, Z., Zhu, L., Zhang, W., and Dou, W., 2007, "Backscattering cross section of ultrawideband antennas", *IEEE Antennas and Wireless Propagation Letters*, **6**, pp. 70-73.

[10] Dardari, D. and D'Errico, R., 2008, "Passive ultrawide bandwidth RFID", *Global Telecommunications Conference, IEEE Globecom*.